The Astrophysical Journal, 885:138 (10pp), 2019 November 10 https://doi.org/10.3847/1538-4357/ab4882

Steady Electron Runaway Model SERM: Astrophysical Alternative for the Maxwellian Assumption

J. D. Scudder
Department of Physics and Astronomy, University of Iowa, Iowa City, IA 52242, USA
Received 2019 July 6; revised 2019 September 24; accepted 2019 September 25; published 2019 November 8

Abstract

A Steady Electron Runaway Model (SERM) is formulated describing plasmas in the astrophysical "condition" having finite (rather than infinitesimal) Knudsen number, $\mathbb{K}_{\rm Pe}$, suggesting an omnipresent leptokurtic, nonthermal, and heat-conducting electron velocity distribution function (eVDF) as the replacement for the Maxwellian ansatz typically made. The shape parameters of SERM's eVDFs are functionals of the local dimensionless electric field, $\mathbb{E}_{\parallel}$, shown to be nearly interchangeable with the pressure Knudsen number, $\mathbb{K}_{\rm Pe}$. The eVDF is determined by the total density and pressure, heat flux, and $\mathbb{E}_{\parallel}$ with the Maxwellian as a special case when $\mathbb{E}_{\parallel} = 0$. The nonthermal part of the eVDF is caused by local and global runaway physics and its density fraction is monotonically dependent on $\mathbb{E}_{\parallel}$. SERM explains the distinguishable conduction band of suprathermal electrons to be the result of the inhomogeneities of astroplasmas that require $\mathbb{E}_{\parallel} \neq 0$ to enforce quasi-neutrality. SERM shows that the direction of the heat flow should be that of $E_{\parallel}\hat{\boldsymbol{b}}$. Almost all reported space age correlations among the shape parameters of the solar wind eVDF are reproduced by this modeling, including scaling of: (i) nonthermal spectral break energy, and (ii) partition of suprathermal density and partial pressure, with solar wind speed. SERM, together with eVDF observations, indirectly bracket $0.2 < \mathbb{E}_{\parallel}(1\ \mathrm{au}) < 0.65$, producing a steady-state eVDF, consistent with in situ (i) heat flows, (ii) *strahl* pitch angle features in high-speed winds, (iii) $J_{\parallel} = 0$, and (iv) non-negative probability at *all* velocities. Because finite $\mathbb{K}_{\rm Pe}$ is the identified prerequisite for SERM modeling, nonthermal eVDF's are expected nearly everywhere in astrophysics where $\mathbb{K}_{\rm Pe} > 0.01$.

Unified Astronomy Thesaurus concepts: Non-Gaussianity (1116); Stellar coronal lines (308); Solar coronal heating (1989); Solar coronal lines (2038); Solar wind (1534)

1. Local Thermodynamic Equilibrium (LTE): Choice or Convenience?

Hidden in many inferences in astrophysics are assumptions about the nature of the collisional regimes where the radiation field was last influenced prior to detection (Dudík et al. 2017; Dzifčáková et al. 2018). A common assumption involves the population of states, which, in the absence of knowledge to the contrary is assumed, *for want of other choices*, to be Maxwellian with density and temperature as parameters. This type of inversion is used to produce impressions of the temperature in plasmas far removed from the observer. A rather general argument is presented here that this mode of inverting photon information has a systematic bias by presuming the Maxwellian eVDF of the LTE when inferring the population of states involved in the line's formation. A suggested alternative is presented based on this paper's Steady Electron Runaway Model (SERM).

Modeling astrophysical plasmas often involves solving the fluid-scale magnetohydrodynamical (MHD) equations. Within the derivation of the MHD fluid equations from the kinetic equations and their closure are further hidden assumptions of LTE (Hazeltine & Walbroeck 2004) that are generally unwarranted on the same large scales of the modeling. These hidden assumptions also preempt consideration of non-LTE types of physics from occurring in such models (Scudder 1992; Meyer-Vernet et al. 1995). Barring improvements that do not make these small Knudsen number LTE approximations, this compromised modeling continues (Scudder 2019a).

To move beyond these (hidden) reliances on LTE requires the formulation of an alternative that challenges the likelihood that the Maxwellian eVDF is the most likely one to occur in the regions under study. To be sure, considering this possibility faces considerable resistance best redressed by studying plasmas with in situ experimental access, such as the solar wind as presented here. There finite $\mathbb{K}_{\rm Pe}$ is clearly common, and this paper argues that this parameter (or its dimensionless parallel electric field cousin) is the central index of the importance of non-Maxwellian eVDF's that is explored in this paper.

The present calculation and its comparison with solar wind measurements furthers the description of transport in plasmas with finite Knudsen number, $\mathbb{K}_{\chi}$, quantitatively defined by

$$\mathbb{K}_{\chi} \equiv \hat{\boldsymbol{b}} \cdot \nabla \ln \chi\lambda_{\rm mfp} \simeq \frac{\lambda_{\rm mfp}}{L}, \tag{1}$$

where $\hat{\boldsymbol{b}}$ is the local magnetic field-aligned unit vector. A fully defined Knudsen number associated with χ depends on the mean free path for scattering, $\lambda_{\rm mfp}$, and the magnetic field-aligned scale, L, of χ. The pressure profile usually has the steepest gradient, determining the shortest transport scale L; it thus determines the relevant $\mathbb{K}_{\rm Pe}$ for the mean free path over scale that enters as a small perturbative parameter in Chapman–Enskog closures (Chapman 1916; Enskog 1917), which are also discussed in Chapman & Cowling (1939), Rossi & Olbert (1970), Fitzpatrick (2004), and Zank (2014). Spitzer and Braginskii use slightly different versions of these expansions (Spitzer & Harm 1953; Braginskii 1965).

Between 0.3 and 5 au the observed solar wind plasma electrons possess $\mathbb{K}_{\rm Pe} \simeq O(1)$. At 1 au $d\mathbb{K}_{\rm Pe}(1\ \mathrm{au}, U)/dU > 0$ (Scudder 2019b). In all speed states of the wind "ubiquitously nonthermal" eVDF have been observed over the last 50 yr.

Being nonthermal, the observed eVDF's possess *kurtosis*, which measures its departure from a local Maxwellian of the same density and mean energy. This kurtosis is of a special type: *leptokurtic*, meaning that the nonthermal signature is exhibited by overpopulated high-energy wings on the VDF, rather than under populated tails that form the *platykurtic* type.

The observed leptokurtic, subsonic eVDF's also support velocity space skewness predominantly at suprathermal energies, determining a net heat flux moment that is generally outwardly directed along $\hat{\boldsymbol{b}}$ in the undisturbed wind. The heat is dominated by energy fluxes at suprathermal energies accompanied by weaker counterposed fluxes from the higher density, but lower mean-energy thermal electrons. Routinely empirical heat flows $q_{\|}$ have been measured, while the same eVDF does not draw electrical currents parallel to $\hat{\boldsymbol{b}}$; in this situation $J_{\|} \simeq 0$, and the electron fluid as a whole is consistently observed moving with no relative velocity to the solar wind ions (Feldman et al. 1975), while supporting a coherent heat flow, $q_{\|}$.

This empirical result demonstrates that predicting heat flow in the plasma requires descriptions that predict the nonthermal partial density fraction of the eVDF (first tracked in the fourth or kurtosis moment). Systems, usually closed at the third moment (Chapman–Enskog perturbative expansion about local Maxwellians), have no chance of describing heat flow physics that is experimentally observed inside of 5 au.

The observed ubiquitous non-thermals conduct heat and cooperate with low-energy electrons to achieve a $J_{\|} = 0$, quasi-neutral, hydrodynamic expansion of the solar wind (Montgomery et al. 1968; Feldman et al. 1975). In this respect the solar wind non-thermals act like an *omnipresent electrical and thermal conduction band* of the plasma, performing a role parallel to that in metals. The recent demonstration of the importance of the plasma specific *thermal force* (Scudder 2019b) completes this identification, identifying the electric and heat flow resistances that allow a magnetic field-aligned force balance in the ion rest frame. In making this identification the constraints on $\mathbb{E}_{\|}$ introduced nearly a century ago for quasi-neutrality in stellar atmospheres, (Pannekeok 1922; Rosseland 1924), must now include the quasi-neutrality demands made on force balance caused by the electrical corollaries of heat transport.

Force balance in the plasma requires that quasi-neutrality and transport physics are not conceptually separable, as shown by the dimensionless Generalized Ohm's Law (GOL; Rossi & Olbert 1970); organized in the usually descending order of importance it takes the form:

$$\mathbb{E}_{\|} = \mathbb{K}_{\rm Pe}/2 + \mathbb{TF}_{\|} + \mathcal{I}. \tag{2}$$

New terms for our discussion are $\mathbb{E}_{\|} \equiv E_{\|}/E_{\rm D}$, $\mathbb{TF}_{\|}$, the *dimensionless thermal force*, (Braginskii 1965; Fitzpatrick 2004; Scudder 2019b), and $\mathcal{I}$ the placeholder for the suppressed inertial terms. Dreicer's electric field, $E_{\rm D}$, (Dreicer 1959, 1960) provides the normalization for the variables in Equation (2); it is widely accepted as the appropriate yardstick of *non-perturbative significance* for parallel electric fields. The *thermal force* occurs in tandem with any heat flow allowed in the plasma; it is always parallel to the direction of the parallel heat flux. In steady state the thermal force preempts thermoelectric currents that otherwise would attend heat flows. The relative sizes of these terms at 1 au are: (i) $\mathbb{TF}_{\|} \leqslant 20\%\mathbb{K}_{\rm Pe}$ (Scudder 2019b) and (ii) $\mathcal{I} \simeq \mathcal{M}_e{}^2(\mathbb{K}_{\rm ne} - 2)$ (see Appendix C), where the electron thermal Mach number, $\mathcal{M}_e \equiv U/w_e$, is only 0.2 at 1 au and lower inside that radius. Thus, Equation (2) can be estimated above the base of the corona out to 1 au to be in the range:

$$\mathbb{E}_{\|} = \frac{\mathbb{K}_{\rm Pe}}{2}(1 + {\rm O}(|<25\%|) - {\rm O}(|<0.05\%|)). \tag{3}$$

These estimates show that generally $\mathbb{E}_{\|} > \mathbb{K}_{\rm Pe}/2$, and that the thermal force correction augments $\mathbb{E}_{\|}$ (Scudder 2019b) relative to any estimate based on the pressure Knudsen number alone. From this the general force balance of GOL (Equation (2)) comes the conceptually useful relation

$$\boxed{\mathbb{E}_{\|} \simeq \mathbb{K}_{\rm Pe}/2}, \tag{4}$$

implying *finite* $\mathbb{K}_{\rm Pe}$ always means *finite* $\mathbb{E}_{\|}$. In turn, finite $\mathbb{E}_{\|}$ implies that $\mathbb{K}_{\rm Pe}$ is non-perturbative.

Perceptions of Knudsen numbers in remote plasmas are now transferable to the size of the dimensionless parallel electric field, $\mathbb{E}_{\|}$ in these same locales. With this realization, perturbatively finite $\mathbb{E}_{\|}$ are understood to be commonplace, which implies that Dreicer's work about a peculiarly plasma effect, the occurrence of *runaways* (Dreicer 1959, 1960) at any finite $\mathbb{E}_{\|}$, is directly and widely relevant to astrophysical transport physics. By contrast the weak gradient premise of LTE presumes perturbative $\mathbb{K}_{\rm Pe}$, $\mathbb{E}_{\|}$, *ensuring* a transport regime unaffected by runaway physics (see Spitzer 1962).

The speed dependence of Coulomb scattering permits a positive feedback situation in the presence of a finite $\mathbb{E}_{\|}$ in which electrons of sufficiently high kinetic energy gain more energy from the field than they lose scattering off of background plasma particles. This locally secular process is called *runaway*. The kinetic energy threshold for this process depends inversely on $\mathbb{E}_{\|}$; accordingly this process affects fewer and fewer electrons when $\mathbb{E}_{\|} \to 0$, the condition for approaching LTE. Thus, perturbative transport about LTE is indeed consistent ignoring runaways; the problem is no longer consistent when a recipe derived for LTE is used for decidedly non-LTE plasmas as occur routinely in astrophysics.

In Spitzer's discussion (that is restricted to perturbative departures from LTE) Equation (2) reduces to $\mathbb{E}_{\|}$ balancing the $\mathbb{TF}_{\|}$ friction, as Spitzer–Härm assumed $\mathbb{K}_{\rm Pe}^{\rm Spitzer} = 0$ (see Equation (25) in Spitzer & Harm 1953).

For more general astrophysical plasmas than those considered by Spitzer, the inertial terms are still usually small, but now GOL (Equation (2)) is a balance between the three, generally non-perturbative forces of inhomogeneity [$\mathbb{E}_{\|}$, $\mathbb{K}_{\rm Pe}$, $\mathbb{TF}$]. However, because GOL is a conservation law, it must be true even when $\mathbb{K}_{\rm Pe}$ is non-perturbative. *This is the new regime of transport physics required for astrophysical plasma steady states made inhomogeneous by gravity, rotation, and radiation.*

The implication of this new transport regime embedded in the SERM model presented here is the unavoidable transport of global particles launched into runaway across the system, coupled with the local conditions required by quasi-neutrality. The possibility of a *global* stationary state in these conditions is motivated by over 50 yr of solar wind observations.

The commonly occurring finite size of $\mathbb{K}_{\rm Pe}$ distinguishes astrophysics as having plasma transport quite distinct from that in LTE plasmas, assumed by Chapman, Enskog, Spitzer, and

Braginskii formulations; global and local access (Scudder & Olbert 1979) must be integrated into the transport description to generate a more realistic, steady macroscopic description of the heat flow. SERM represents an initial attempt to do this.

2. Runaway and Steady State?

2.1. Runaway Morphology

Any finite $\mathbb{E}_{\|}$ drives *part* of the plasma's eVDF into runaway, inducing a subset of the local electrons into *partial* runaway; they should be viewed as an under damped (UD) response, where more energy is gained from the emf than lost by scattering off background ions (Dreicer 1959, 1960). In Dreicer's formulation such partial runaways occur for *finite* $\mathbb{E}_{\|} \ll 0.43$, even before catastrophic bulk runaway, characterized by large parallel currents, that disrupted early fusion lab experiments. As argued by Dreicer, the complementary group of overdamped (OD) lower kinetic energy complements of velocity space was quasi-ohmic and significantly impacted by Coulomb drag. The boundary between UD and OD electrons is a mathematical separatrix *implicitly* defined by the size of $\mathbb{E}_{\|}$. (Dreicer 1960; Fuchs et al. 1986).

In the presence of finite $E_{\|}$ the UD and OD electron trajectories are separated in pitch angle and speed by a pear-shaped velocity space separatrix surface, enclosing the ion rest frame velocity (Fuchs et al. 1986). The minimum kinetic energy $\mathcal{E}$ on the separatrix is found along the direction of $-eE_{\|}\hat{\boldsymbol{b}}$, defined in thermal units as

$$\varpi^2 \equiv \frac{\mathcal{E}}{kT_{\rm th}} \equiv \frac{\alpha}{\mathbb{E}_{\|}}, \tag{5}$$

where $(kT)_{\rm th}^{-1} = -d \ln f_{\rm OD}/dE$. Dreicer estimated $\alpha \simeq 3$ (Dreicer 1959), but recent Langevin improvements (Fuchs et al. 1986) suggest its value is between $1.42 < \alpha < 3$. Solar wind data at 1 au (not shown) suggest $\alpha \simeq 2$.

Approaching the regime of thermodynamic equilibrium, the predicted runaway boundary given by Equation (5) recedes to infinity as $\mathbb{E}_{\|} \simeq \mathbb{K}_{\rm Pe} \downarrow 0$ in this gradient-free regime. There all electrons are OD by collisions; global "runaway" trajectories do not occur; this is the regime where Maxwellians are expected. Regimes where $\mathbb{K}_{\rm Pe} \simeq \mathbb{E}_{\|} \rightarrow 0$ are very rare in inhomogeneous astrophysical plasmas (Scudder & Karimabadi 2013), explaining the extremely rare occurrence in natural plasmas of truly Maxwellian eVDFs.

A finite population of UD runaway particles accompanies a finite $\mathbb{E}_{\|}$ (Dreicer 1959, 1960). Phase-space characteristic flow lines for electrons start and remain either (i) outside or (ii) inside the separatrix. Those outside are UD by collisions and are increasingly accelerated by $E_{\|}$ away from their initial locale, while the group of low-energy characteristics starting within the separatrix remain inside it, and are OD by Coulomb collisional losses. Described at the fluid level, the OD population comes to a Stokes frictional equilibrium, drifting with respect to the ion rest frame displaced in the direction of the applied force, keeping the observed nearly Maxwellian form via Coulomb collisions (Dreicer 1959, 1960).

The bifurcation of velocity space afforded by this Coulomb-enabled separatrix allows SERM's eVDF to have a spectrally different electron thermal and suprathermal phase space; this spectral break is also predicted to occur at a boundary specified by $\mathbb{E}_{\|}$. This explanation is totally consistent with that shown previously integrating a model kinetic equation in a specific context, (Scudder & Olbert 1979).

2.2. How So, Steady Runaway?

Dreicer's focus was explaining transient responses of laboratory plasmas when experiencing large field-aligned electric fields. SERM as an astrophysical model addresses "steady runaway," which would appear to be an oxymoron.

The basic difference is that the laboratory plasmas tended to have only mean free path and experiment scales in them, such that runaway across $\lambda_{\rm mfp}$ usually meant the UD particles were hitting the experimental "walls," thus representing large currents from the plasma to their boundaries and leaving the ions unshielded, making time dependence guaranteed. In addition, these early experiments did not traverse strong variations in background properties before the particles heated the vacuum chamber boundaries.

In the astrophysical circumstance the scale of the box (system) is many $\lambda_{\rm mfp}$; across these large scales the "external forces" of the plasma are often organized with scale lengths of their own, such as those caused by magnetic fields, electrical potentials, gravity, rotation, pressure gradients, or concentration gradients. These circumstances admit the possibility that UD populations from many runaway sites can be in communication across these intermediate scales, and that the background forces and collisional frequency variation across them could be instrumental in assisting recirculation of UD particles on these intermediate scales. Such recirculation would be necessary for return current channels to form or be a concomitant part of the local runaway morphology that could produce a global view where steadiness and quasi-neutrality were possible.

The experimental evidence ($J_{\|} = 0$, $n_e \simeq \Sigma Z_i n_i$, $U_e = U_i$ in the solar wind suggests that this has happened, despite the very large $\mathbb{E}_{\|}$ values that are implied by the observed gradients in the medium (Scudder 2019b). While significant time dependence occurs in astrophysical systems, considerable correspondence between data and theory has been exhibited assuming astrophysical steady systems are realized ($\partial/\partial t = 0$).

2.3. The Gauntlet: Steady Runaway

In recognition of the likely hesitancy to accept the possibility of runaway physics embedded in a steady description, considerable effort is expended below to see if such a model's predictions are contradicted by the vast volume of solar wind data compiled with in situ interplanetary observations. The short summary is that no contradiction has yet been identified, while nearly every known correlation in the electron properties of the eVDF is provided an explanation given if runaway physics is respected and its implications are followed to their conclusions. Because many of these properties have been archived repeatedly by multiple experimental groups and SERM's explanation for their behavior is the first in 50 yr, SERM is worthy of further consideration.

3. Challenges for SERM

Six immediate questions the SERM model must answer are how can the "transient" runaway concept (i) produce long-term correlations between the suprathermal density fraction and the bulk speed at 1 au; how can finite and thus strong $\mathbb{E}_{\|}$ (ii) be

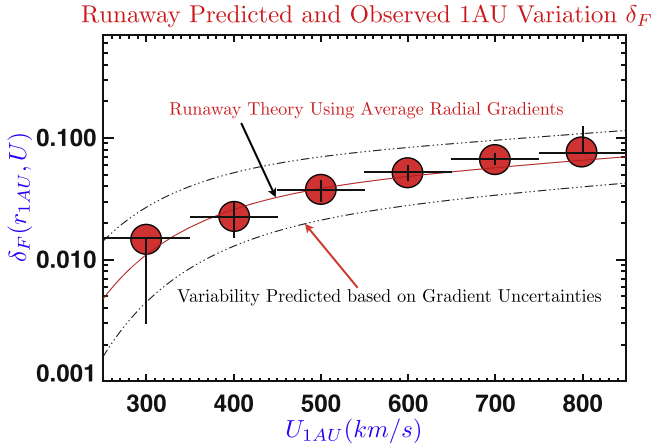

Figure 1. Suprathermal density fraction vs. solar wind speed U at 1 au: δ_F(predicted) vs. δ_F(observed), $\simeq 0.59 n_h/n_c$ as argued in Appendix B. Data are adapted from (Feldman et al. 1979). The dashed–dotted lines indicate the possible variability of δ_F expected from the inferred uncertainty of $\mathbb{E}_{\|}(U, 1\ au)$ allowed by the reported electron radial pressure profiles.

consistent with, rather than disrupt, quasi-neutrality by runaway production; (iii) enforce zero parallel current in the manner observed with the thermals always lagging the ions; (iv) sustain a steady heat flow of the appropriate size and direction; systematically produce ubiquitous (v) leptokurtic eVDF; and (vi) explain other quantitatively well known, persistent correlations among the shape properties of the eVDF.

3.1. Steady

To achieve a steady state, the SERM asserts that the *density fraction implied by the time average of UD transits at all pitch angles and allowable energies must balance the promoted runaway density fraction δ_F lost by that local observer*, yielding a global-local compatibility condition that restates a pervasive quasi-neutrality condition:

$$\int_{\mathrm{UD}(\mathbb{E}_{\|}(\boldsymbol{x}))} f_{\mathrm{UD}}(\boldsymbol{w}, \boldsymbol{x})\, \boldsymbol{d}^3\boldsymbol{w} = n_e \delta_F(\mathbb{E}_{\|}(\boldsymbol{x})), \tag{6}$$

where the limits of integration encompass the phase space *outside* the locally determined velocity separatrix between the OD and UD sub-fluids, and $\boldsymbol{w} = \boldsymbol{v} - \boldsymbol{U}$ is the random velocity of the electron in the ion rest frame with inertial frame bulk velocity $\boldsymbol{U}$. It should be noted that had Equation (6) not been imposed, the incidence of *electron runaway* from s_o, would have had the corollary that the ions at s_o would no longer be shielded, a violation of quasi-neutrality incompatible with a search for a stationary quasi-neutral situation.

The second SERM approach to the steady-state requirement postulates that $J_{\|} = 0$ occurs on the same timescale over which eVDF is measured. This implies that the UD electron number flux in the ion rest frame should represent a neutralizing return current, equal and opposite to the starward OD number flux driven by $E_{\|}$ opposed by significant coulomb resistance. Thus, SERM's second postulate becomes

$$\int_{\mathrm{OD}(\mathbb{E}_{\|})} f_{\mathrm{OD}}(w) \boldsymbol{w} \cdot \hat{\boldsymbol{b}}\, \boldsymbol{d}^3\boldsymbol{w} = -\int_{\mathrm{UD}(\mathbb{E}_{\|})} f_{\mathrm{UD}}(w) \boldsymbol{w} \cdot \hat{\boldsymbol{b}}\, \boldsymbol{d}^3\boldsymbol{w}, \tag{7}$$

where the limits of integration are complementary, but together cover all of velocity space. This condition enforces no charge polarization along field lines and hence no space charge changes in time along them.

3.2. Trial Function Approach

Ideally, a solution to the kinetic equation that meets the conditions of Equations (6) and (7) is desired. An alternate approach taken here is to suggest a plausible trial function f^0 that meets these integral conditions that have minimal, spatially dependent free parameters that can be constrained by imposing the conservation equations of the two-fluid system, including thorough consideration of important collision terms. This full program involves demonstrating that such an approach is closed (J. D. Scudder 2019, in preparation).

3.3. Symmetric Trial Function: f^0

Fortunately, as is developed below, the building of this trial function can proceed and be tested in two parts based on its velocity space symmetry. The transport signatures require a trial function with anti-symmetric parts along the magnetic field. The symmetric parts are the total contributors to the density, the dominant parts of the pressure, and kurtosis tensors, to name just a few. The heat flow moment depends on both the existence of the anti-symmetric parts, but also scales with the number density of the electrons that support the heat flow. The trial function for the symmetric parts is denoted f^0, while the total distribution with anti-symmetric parts is denoted f^1.

The usual test function for Spitzer–Braginskii and C-E expansions is the convected Maxwellian; this approach perturbatively seeks to correct this symmetric distribution, producing a heat flow, viscosity etc. The observed heat flux asymmetries are not perturbative corrections to a Maxwellian eVDF.

3.4. Suprathermal Density versus SW State?

Before constructing the mathematical trial function of SERM's choice a first hurdle is to see heuristically if there are enough locally UD electrons predicted to explain the observed nonthermal densities observed in the solar wind as a function of solar wind speed (Feldman et al. 1975, 1978, 1979).

The SERM postulates that steady runaway is only allowed if the steady state remains quasi-neutral (Equation (6)) and becomes the steady-state density fraction observed in the UD energy range,. Also, δ_F must be restored to the same fraction that left according to local runaway theory's prediction. In symbols this becomes

$$\delta_F(\mathbb{E}_{\|}) = \mathbb{D}(\mathbb{E}_{\|}), \tag{8}$$

where $\mathbb{D}(\mathbb{E}_{\|})$ is the density fraction numerically computed to have left the location with $\mathbb{E}_{\|}$ after the separatrix has itself been numerically identified knowing $\mathbb{E}_{\|}$.

It should be noted that when a plasma instrument samples the eVDF at s_o it is actually performing a time average over those electrons whose worldlines happen to pass through s_o and the instrument's passband during the instrument's integration time. In this sense it is integrating over "prehistories" (i.e., characteristics) of particles that have gotten to s_o with the correct arrival time, velocity, and energy for collection. In the OD regime the spatial volume traversed by these trajectories is smaller than those for the UD energy range. All trajectories seen in the local UD energy range are a convolution over a

wide spatial domain and can be thought of as electrons launched into runaway at some $s' \neq s_o$. This condition of quasi-neutrality (Equations (6), (8)) and (7) are constraining the immense freedom otherwise possible in this energy regime.

Equation (8) embeds the essence of the speed dependence of the Coulomb cross section into the transport problem; note that this is not an asymptotic part of this speed dependence but represents a holistic approach to considering the impacts on UD and OD domains at the same time. The balance between these two domains is controlled by the size of $\mathbb{E}_{\|}$. With $\mathbb{E}_{\|}$ being finite there *is* a tradeoff to be made, just as when it vanishes there is not and the UD volume vanishes.

Because Equation (5) scales inversely with $\mathbb{E}_{\|}$, stronger $\mathbb{E}_{\|}$ implies lower kinetic energy thresholds for runaway electrons, resulting in a larger density fraction of UD runaways, δ_F. However, larger $E_{\|}$ produces higher solar wind speeds (Meyer-Vernet 2007), immediately predicting higher suprathermal density fractions, δ_F, should accompany higher flow speeds. *This morphology has been observed for decades* (Feldman et al. 1975, 1978, 1979), *but never explained until the present SERM model.*

The red filled circles in Figure 1 show the long-term correlation at 1 au of the observed suprathermal density fraction, estimated as $\delta_F \simeq 0.59 n_h/n_e$ with solar wind speed, U, where n_h/n_e is the halo fit density fraction (see Appendix B for our rationale). The red curve shows the predictions of the SERM model discussed in this paper, using sketchily available electron radial pressure profiles (Marsch et al. 1989) and the electron momentum equation to determine $\mathbb{E}_{\|} \simeq \mathbb{K}_{\rm Pe}/2$ and then predict the $\delta_F = \mathbb{D}(\mathbb{E}_{\|})$ summarized by the blue curve in Figure 3. The dotted–dashed curves (in Figure 1) suggest compatible limits permitted by the sketchy radial profile data available as a function of U. Figure 1 demonstrates that SERM's runaway picture can supply the observed density fraction of suprathermals routinely observed in the solar wind, as well as their expected interrelationship with solar wind speed.

3.5. Trial Function Choice

SERM seizes on the existence of a bifurcation in the Coulomb physics above a minimal kinetic energy $\mathcal{E}$ to assume that its trial function $f^o = \text{eVDF}^o$ could be *allowed* to be non-perturbatively kurtotic above a prescribed kinetic energy, $\mathcal{E}(\mathbb{E}_{\|})$ solely determined by $\mathbb{E}_{\|}$. At the same time the arguments of Dreicer make a persuasive case that the OD electrons within the bifurcation with $E < \mathcal{E}$ should be strongly influenced by Coulomb scattering and be representable as a convected Maxwellian form. This suggestion has been adopted for f^0 and is shown (with no convection) in Figure 2.

SERM assumes that f^0 has the following plausible properties: (i) is *continuous* at the bifurcation boundary between (OD) thermal and (UD) suprathermal regimes; (ii) *permits a spectral break* at the minimum kinetic energy for runaway $\mathcal{E}$; (iii) the OD population is reasonably assumed to be a *truncated Maxwellian below* $\mathcal{E}$; and (iv) the UD subspace modeled either by: (a) a possibly different Maxwellian; or (b) a power law in speed.

The ubiquitous occurrence and success of the two Maxwellian core-halo models (Feldman et al. 1975), suggests that the proposed function space for f^0 is expansive enough to permit such a distribution if the conservation equations require. Model (a) for the UD part of the eVDF has the wider solar wind database for comparison and will be explicitly developed here.

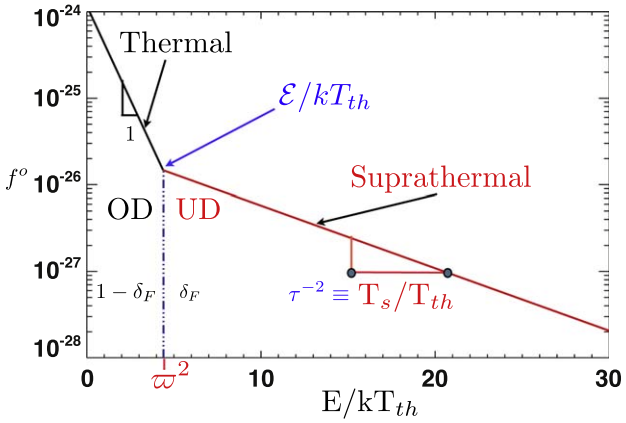

Figure 2. Assumed *non-local* kurtotic *local kinetic energy E* spectrum, $f^0(E)$, compatible with the *local* runaway hypothesis explored in this paper. It possesses a suprathermal density fraction, δ_F, for energies above a break kinetic energy $\mathcal{E}$ with two abutting, truncated, but continuous Maxwellian components with ratios of semi-logarithmic derivatives indicated in the ratio $\tau \equiv \sqrt{T_{\rm th}/T_s}$. The interrelated parameters for the *symmetric shape* of f^0 are ϖ, δ_F, $\mathcal{E}$, and τ, *all* determined by $\mathbb{E}_{\|}$ (see Equations (5) and (11)).

Similar tendencies to those reported here are seen with the power-law model (see Appendix B). This chosen function space for f^0 *allows departures* from a single Maxwellian, but does not enforce any relationship between spectral indices [$T_{\rm th}$, T_s] of the OD and UD regimes; it does build in the runaway theory's $\mathbb{E}_{\|}$ dependence of any possible *hinge* point at $\mathcal{E}$ in the context of Coulomb scattering. When satisfying the global-local constraining equations mentioned above there is no a priori preference in this function space for *leptokurtic* ($T_s/T_{\rm th} > 1$), *platykurtic* ($T_s/T_{\rm th} < 1$), or Maxwellian ($T_s/T_{\rm th} = 1$) forms.

3.6. Why is f^o Isotropic with Runaways?

Dreicer's original suggestion for runaway phenomena gives the impression that the UD electrons in runaways would be found in velocity space to the left of a parabola whose symmetry axis was along $\hat{\boldsymbol{b}}E_{\|}$; more recent discussions by Fuchs and colleagues have shown that the separatrix between OD and UD is a closed elliptical curve, off center about the origin with the same symmetry axis as Dreicer's. This revision clearly establishes that those particles launched from the separatrix are inserted in all of 4π, albeit with intensity variations that favor the force direction of the field on the electrons.

It is important to explore why the local runaway's preferential injection toward the proximate star might be involved in supporting the observed quasi steady state *near isotropy* of the nonthermal eVDF. If all collisions were elastic, a returning, originally stellar-headed runaway would have a comparable kinetic energy and sign-reversed cosine of pitch angle as when it left. The plasma at s_o is almost collisionally transparent to their transit, allowing "passage through" s_o as UD particles within the suprathermal *pattern* of Figure 2, but now heading toward the astropause.

Thus, suprathermal runaway in *near* symmetry in the presence of a preferred orientation of the accelerating force is a zeroth-order manifestation of the nearly reversible recirculation of the UD particles in the star's increasing magnetic field and that the sites of runaway promotions occur on both sides of the observer's position. The collisions experienced can change the runaway's returning pitch angle and can also cause some

starward-headed runaways to precipitate into the chromosphere. Away from $\mathcal{E}$, almost all pitch angles are equally eligible for promotion into stellar runaway, leading to a similar range of pitch angles occupied for those mirroring runaways. The OD particles are maintained nearly isotropic by strong collisions, and remain nearly so if their ohmic drift is subsonic (Dreicer 1959, 1960).

Directional bias is still required to support the counter-drifting OD and UD components that implement zero current, heat flux, and thermal force. These are all transport signatures involving odd velocity space moments of the eVDF. In terms of spherical harmonics, these effects would be represented by admixtures of odd spherical harmonics $Y^m_{2\ell+1}$ that are orthogonal to the spherically symmetric description of the f^0 shown in Figure 2. As odd harmonics they do not contribute to the density of either UD or OD subcomponents; this permits reasonable comparisons of even-moment quantities like partial densities, pressures, or kurtosis between observations and an eVDF based on f^0 without its odd-moment transport contributions included.

4. SERM Function Space f^o

The function space f^0 respects runaway physics in several ways: (i) it provides for a spectral change at the minimum energy, $\mathcal{E}$, for runaways to be possible; and (ii) acknowledges the much stronger role of Coulomb collisions inside the separatrix that Dreicer argued would lead that part of the eVDF being modeled as a convected Maxwellian. These transport signatures will be addressed in f^1; for the present f^0 takes the analytic form

$$f^o(\tau, \varpi, x) = \gamma\{exp^{-x^2}(1 - \Theta(x - \varpi)) + \exp^{-x^2\tau^2+\varpi^2(\tau^2-1)}(1 - \Theta(\varpi - x))\}, \quad (9)$$

where $x^2 = E/kT_{\rm thermal}$, τ, and ϖ^2 are defined in Figure 2 and Equation (5); $\Theta(g)$ is the Heaviside step function. This function space choice has a fractional suprathermal density δ_F that is constrained by the identity

$$\frac{\delta_F}{1 - \delta_F} \equiv \frac{\int_{\mathcal{E}(\mathbb{E}_\parallel)}^{\infty} f^0(\tau, \varpi, v)v^2dv}{\int_0^{\mathcal{E}(\mathbb{E}_\parallel)} f^0(\tau, \varpi, v)v^2dv} = \mathcal{H}(\varpi, \tau). \quad (10)$$

Runaway physics suggests the size of δ_F is already determined by $\mathbb{E}_\parallel$ via steady-state Equation (8). Used with Equation (10) it becomes clear that τ is itself only function of $\mathbb{E}_\parallel$:

$$\boxed{\frac{\mathbb{D}(\varpi^{-2})}{1 - \mathbb{D}(\varpi^{-2})} = \frac{e^{-\varpi^2}}{\tau^3}\frac{\sqrt{\pi}\,\mathrm{Erfcx}(\varpi\tau) + 2\varpi\tau}{\sqrt{\pi}\,\mathrm{Erf}(\varpi) - 2\varpi e^{-\varpi^2}}}, \quad (11)$$

where $\varpi^2 = \alpha/\mathbb{E}_\parallel$ and where $\mathrm{Erfcx}(y) \equiv e^{y^2}\mathrm{Erfc}(y)$. Because ϖ and δ_F are both functions of $\mathbb{E}_\parallel$, Equation (11) implies that τ is a function of $\mathbb{E}_\parallel$ that numerically is shown to be one-to-one by comparing the red and blue curves in Figure 3. The red curve for the ratio of OD and UD mean energies $\overline{E_s/E_{\rm th}} \simeq T_s/T_{\rm th} = \tau^{-2}$ is seen to be one-to-one and anti-correlated with δ_F, and, therefore one-to-one and anti-correlated with $\mathbb{E}_\parallel$. The green eVDF break point energy $\mathcal{E}$ curve is also inversely correlated in a one-to-one manner with δ_F because of Equation (5).

Because τ is operationally found to be less than unity, implying $\overline{E_s/E_{\rm th}} \geqslant 1$, implementing these SERM constraints has also just *correctly* inferred the *lepto-* versus *platy-* kurtic property commonly observed in the solar wind eVDF, with $T_{\rm halo} > T_{\rm core}$ in the solar wind eVDF (Feldman et al. 1975).

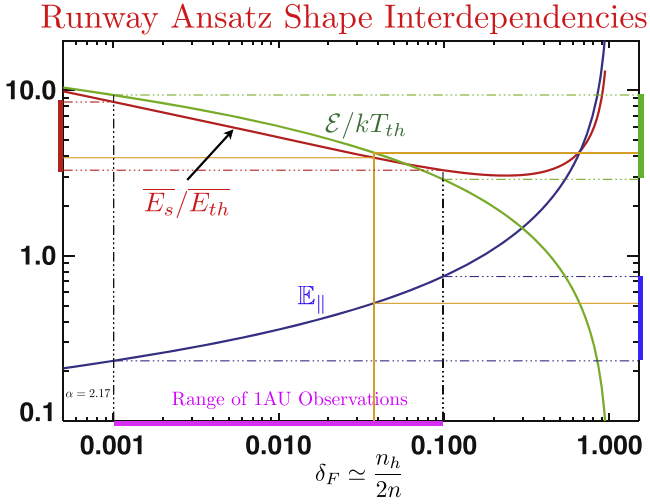

Figure 3. Behavior implied by Equation (11) for the expected correlated nonthermal properties of of the SERM eVDF at a given runaway number density fraction, δ_F at the specified dimensionless parallel electric field $\mathbb{E}_\parallel$ predicted by the runaway (Fuchs et al. 1986). All parameter curves crossed by a given vertical line are correlated properties in the same VDF. Ranges of solar wind electron parameters, from decades of observations for properties with a given colored curve, are shown by the thick colored bars on the plot perimeter.

Conceptually, Equation (11) has established that all of the shape parameters of f^0 are functions of the $\mathbb{E}_\parallel$. This implies there are many correlations between and among the parameters that determine f^0 that are now understandable by solving for $\mathbb{E}_\parallel$ in terms of one of these shape parameters and inserting this dependence for that of the electric field in another shape variable, generating an interrelationship free of any outward dependence on $\mathbb{E}_\parallel$.

At the two-fluid level the parallel electric field is essentially determined by the electron momentum equation, including the thermal force. If $E_\parallel$ is chosen to be consistent with that force balance, the ensuing chains of shape parameters for f^0 are functionally entrained to other moment variables of the plasma two-fluid description. This bodes well for attempting a closure via SERM within the properly closed two-fluid equations (J. D. Scudder 2019, in preparation). The most troubling problem for closures is securing a sufficiently flexible but defensible velocity space functional description that remains positive, with spatially varying shape parameters computable from the moments of the species equations (see Scudder 2019a).

The observed range at 1 au of these *shape parameters* that also determines the nonthermal properties of the solar wind electrons is shown by the thick colored bars along the perimeter of Figure 3. They reveal the following:

(1) The magenta colored bar indicates the range of δ_F seen at 1 au over 14 yr of solar wind conditions (Feldman et al. 1975, 1978, 1979).
(2) The vertical dashed lines from these extremes intersect the red ratio of mean energies curve, predicting an expected range of $T_s/T_{\rm th}$ (indicated by the thick red vertical segment left axis) that should attend the observed range of δ_F. The extent of this SERM inferred range for $T_s/T_{\rm th}$ at 1 au nearly perfectly predicts that observed in the solar wind literature.

(3) With this procedure higher $T_s/T_{\rm th}$ ratios are suggested to accompany lower δ_F, an observed property known since the 1970s, but never explained.
(4) SERM also suggests the observed 1 au range (4–7) of $\mathcal{E}$ indicated by the olive bar (Feldman et al. 1978).
(5) SERM's suggested range for $\mathbb{E}_{\|}$(1 au) is indicated by thick blue segment on the right edge of Figure 3, using the magenta observed range of δ_F as before. The few estimates of $\mathbb{E}_{\|}$(1 au) in the literature are in this range (Scudder 1996a, 1996b; Issautier et al. 1998). A parallel study using *Helios* data fully confirms the SERM suggested range of $\mathbb{E}_{\|}$ (Scudder 2019b).
(6) The bulk speed dependence from *Helios* of $\mathbb{E}_{\|}(U)$ has already been used in the red curve for $\delta_{F_{\rm obs}}$ versus $U_{\rm obs}(\mathbb{E}_{\|}(U))$ in Figure 1.

The highly reproducible and correlated values of $\tau(U)$, $\delta_F(U)$, $\mathcal{E}(U)$ in 1 au solar wind data are explained by SERM through their common ties to $\mathbb{E}_{\|}$ and U to $\mathbb{E}_{\|}$. The organization with solar wind speed can be viewed as determined by the requisite $\mathbb{E}_{\|}(U)$ required for a quasi-neutral wind of speed U implicit in Figure 1.

These quantitative explanations at 1 au of the solar wind eVDF properties and their interrelationships and reproducibility of the ubiquitous leptokurtic eVDF are *the first of their kind since their initial reports 50 yr ago* (Montgomery et al. 1968).

5. SERM's Zero-current Condition

However, the full predictive capability of SERM requires consideration of the determinants of the odd velocity moments that control the parallel *thermal force* $\mathbb{TF}_{\|}$, parallel *current* $J_{\|}$, and parallel heat flux $q_{\|}$, all of which require odd harmonic content not present in f^o.

The second global-local premise of SERM (Equation (7)) demands that the eVDF in the UD domain in steady state provide a *local return current* to enable $J_{\|}=0$ after first considering the OD response to the forces they feel. That this requirement is non-trivial can be understood better by looking at the response of the OD electrons within the separatrix. In the absence of gravity the microscopic force is supplied by the omnipresent $E_{\|}$ that drives the OD electrons, against the Coulomb drag provided by the ions (and weakly by the UD electrons) until they come to a time stationary steady drift with no net force, lagging the ions.

Dreicer studied the related problem of electrons flowing through ions under an applied $E_{\|}$ and showed that a final steady state could be found for $\mathbb{E}_{\|}<0.43$ in which the electrons were moving steadily at a thermal Mach number $\mu=\hat{\boldsymbol{b}}\cdot(U_e-U_i)_{\|}/w_c\propto-\mathbb{E}_{\|}$. This motion is toward the Sun in the ion frame and is precisely the reported behavior of the core drift (Feldman et al. 1975) with reported $\mu\simeq-O(V_a/w_c)$.

The return current requirement of SERM in Equation (7) has five corollaries: (i) $J_{\|}=0$; (ii) ensures the star does not charge; (iii) makes the UD population discernible in the eVDF *if only by its counterposed drift to that of the OD population*. Together with SERM's Equation (6) the fourth notable achievement is (iv) that the lowest-order eVDF consistent with Coulomb physics is skewed, carrying a non-perturbative heat flow, $q_{\|}$, a result that follows from the finding that the lowest-order eVDF is kurtotic for finite $\mathbb{E}_{\|}$. With SERM's specific preference for leptokurtic shapes comes the fifth notable result: (v) the heat flow is suggested to be parallel to the direction of $E_{\|}$ and it is algebraically determined by the difference of enthalpy fluxes of the OD and UD populations, a pattern noted in the data inventory of solar wind data (Feldman et al. 1975).

In this way the SERM model provides the first quantitative theoretical explanation for the ubiquitous, nonthermal, counter-drifting, core-halo type solar wind distributions reported since 1968 (Montgomery et al. 1968; Feldman et al. 1975, 1978, 1979). Subsequent steps in SERM's direction include a model kinetic equation (Scudder & Olbert 1979), enhanced kinetic equation modeling (Olbert 1983), and Monte-Carlo calculations (Landi & Pantelinni 2003).

SERM relates nearly all signatures in the nonthermal eVDF to the size of $\mathbb{E}_{\|}$ in the self-consistent solar wind problem. This connection between velocity space features and macroscopic moment quantities is critical for building a successful closure (J. D. Scudder 2019, in preparation).

5.1. SERM: Positive eVDF, Transport, Implementation

SERM's approach to this problem is to extend the function space so that $f^o\rightarrow f^1$, where (i) f^1 has odd moments, while (ii) is constrained to everywhere be a positive definite eVDF with $J_{\|}=0$, without enforcing $J_{\|}=0$ as a perturbative statement. Considerable hints that our process can describe nature are found in the core-halo parameterization of the solar wind eVDF (Feldman et al. 1975). The thermals and suprathermals were modeled with their own (anisotropic) convecting Maxwellian forms. It was demonstrated that the thermals and suprathermals drifted in opposite directions along the magnetic field in the ion frame of reference, compatible with satisfying zero current. The cross-field drifts of the thermals, suprathermals, and ions were shown to be the same within errors.

5.2. Toward Odd Moments, Closure with $f^1>0$

When the transport construction of SERM is complete, the eVDF will look like the core-halo-strahl eVDFs that have been observed in the solar wind. Two feasibility studies that suggest the transport description is near involve (I) production of heat flows like those observed; and (II) identifying conditions when SERM eVDFs possess strahl like features.

(I) Above we have shown that the shape parameters of f^0 exclusively favor leptokurtic nonthermal f^0. SERM illustrates how the microscopic forces produce different results inside versus outside of the velocity space separatrix. With the possibility of differential responses of UD and OD required when $\mathbb{E}_{\|}\neq 0$, there is in general a heat flow implied if this response enforces $J_{\|}=0$ (Scudder 2019b). SERM supports a heat flow like that observed in the core-halo model (Feldman et al. 1975), well approximated by

$$\begin{aligned} q_{\|} &= \frac{5}{2}n_h\Delta U_{h,/\|}k(T_h-T_c)\\ &= -\frac{5}{2}n_c\Delta U_{c,\|}k(T_c-T_h), \end{aligned} \tag{12}$$

which is only non-zero if the composite eVDF is kurtotic and only has the correct sense with the numerically integrated heat flow if the eVDF is leptokurtic with $T_h>T_c$ and $\Delta U_{h,\|}$ leads the ions. All these apparently arbitrary free parameters in Equation (12) are predicted by SERM.

Although the SERM model will have a structure like this, the missing ingredient(s) are the constraining equation(s) for the drifts of the OD electrons in the ion's rest frame. These

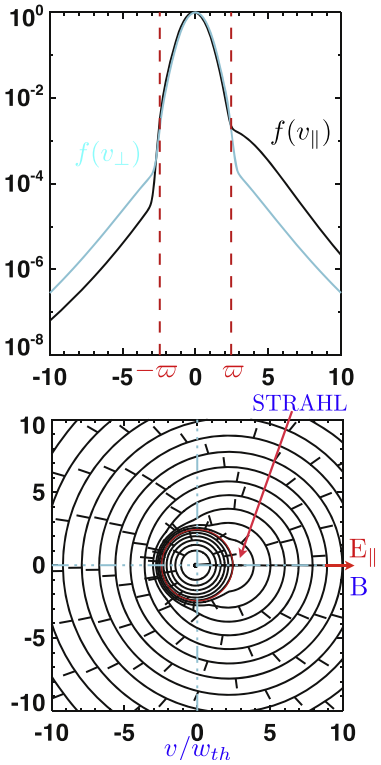

Figure 4. SERM eVDF in high-speed 1 au conditions. Note the field-aligned feature akin to the reported strahl. "Tags" on contour lines indicate the downhill direction.

equations with closure are forthcoming (J. D. Scudder 2019, in preparation).

(II) A common feature of the highest-speed winds is an astropause-headed narrow pitch angle enhancement in the eVDF at intermediate energies, called the *strahl* or ray (Rosenbauer et al. 1977). Figure 4 shows an illustrative SERM f^1 eVDF using high-speed solar wind parameters that are consistent with strahl observations and occurrence morphology. It shows that SERM can predict magnetic field-aligned pitch angle enhancements when the OD electrons are driven hard by the strong $\mathbb{E}_\parallel$ that accompanies higher speed winds at 1 au. The top inset shows eVDF sections (black) along and (cyan) perpendicular to the magnetic field direction, while the bottom inset shows a contour picture (at equal increments) of the skewed nonthermal eVDF sampled in a plane containing the magnetic field made up of both UD and OD populations. The SERM model suggests the indicated strahl feature emerges gradually at 1 au as $\mathbb{E}_\parallel$ increases, a situation synonymous with increasing wind speeds (Scudder 2019b, 2019c) and core counter-drift behavior (Pulupa et al. 2014). This figure also shows, with its more widely spaced contours at higher energies, the leptokurtic character of the eVDF predicted by the SERM model and invariably observed. The displacement of the OD and UD populations in opposite directions along $\hat{\boldsymbol{b}}$ yield zero current and a clear skewness, indicative of heat flow. The displacement at low energies is hard to resolve given the figure size limitations.

5.3. SERM and Exospheric Modeling

SERM is significantly different from the exospheric picture that, while keeping the eVDF positive everywhere, ignores collisions altogether. The exospheric picture identifies positive and negative total energy states with the suprathermal and thermal electron populations, but cannot produce sunward particles in the suprathermal energy range (except by boundary conditions). Nor can it explain why positive energy states should be spectrally different (leptokurtic or platykurtic) from the negative energy states (except by adjusting boundary conditions for this purpose), or explain how the negative energy electrons move nearly with the ions, as observed.

5.4. SERM and Coulomb Collisions

In SERM the Coulomb collisions and finite $E_\parallel$ are included from the outset; together they (i) determine the velocity space separatrix of the eVDF; (ii) explain the segregation of velocity space with distinct properties; (iii) produce different prehistories for UD and OD electrons; (iv) cause the OD electrons inside the separatrix to lag the ions as an overdamped mechanics problem; (v) strain the system's quasi-neutrality by the ohmic response of the OD electrons performing this differential drag; (vi) require the return current of the UD damped particles; (vii) dictate the density fraction of UD particles in steady state to shield the protons; (viii) produce the skewness for the lowest-order heat flux; and (ix) associate *strahl* morphology with $\mathbb{E}_\parallel$ in the high-speed wind at 1 au.

5.5. SERM and Conduction Band

In a similar manner the conduction band in a metal is the zone where global potential differences are resolved, where currents flow until they are resolved, and where heat flows as a corollary of the induced gradients and the finite random speed distributions of the particles. The UD electrons are conceptually the thermal and electrical conduction band of an inhomogeneous fully ionized plasma; the analog of the crystalline lattice is the background ions of the quasi-neutral gas with which there is significant frictional coupling, and where the OD electrons come to a Drude-like equilibrium that through UD return current drifts ensure $J_\parallel = 0$ equilibrium.

6. SERM versus LTE in Astroplasmas?

The predicted eVDF of SERM represents the first kinetic explanation of why the heat flow observed in the solar wind is controlled by suprathermals in the eVDF. This form is totally unexpected in the traditional C-E or N-moment gradient expansions about Maxwellian or bi-Maxwellians. At the same time SERM quantitatively explains the *size* of nearly all nonthermal shape parameters of the observed solar wind eVDF, *including* many mysterious, but ubiquitous correlations between them that have remained unexplained for over 50 yr. SERM also provides a rationale for why zero current is supported with UD electrons leading the ions and OD electrons lagging, rather than the reverse pattern that also satisfies zero current.

SERM's relevance for astrophysical plasmas is assured by the common occurrence of certain plasma parameters that occur in the solar wind and most astrophysical plasmas between the stars: (i) finite pressure Knudsen numbers, (ii) absence of coupling to the radiation field, (iii) flow speeds that are subsonic relative to the electrons, and (iv) temperatures high enough for heat conduction to be competitive in the plasmas energetics. As none of these parameter regimes are especially restrictive, the nonthermal eVDF of SERM should be a common occurrence outside the nominal radii of most stars. At

the very least this possibility should be a routine consideration for the interpretation of the plasma properties in remote photon source regions, the possible dynamics of plasmas in these source regions, and for the types of plasma dynamics that are permitted. This domain has a number of theoretical surprises (Scudder 1992; Meyer-Vernet et al. 1995) compared to plasma predictions predicted by LTE closures that have until recently heavily biased the large scale pictures of these regimes.

Useful comments were made on an early draft of this paper by R. Merlino, U of Iowa. The energetic support for innovative thrusts in research by NASA-SMD is sincerely appreciated. Editorial assistance by SED for this research was also extremely helpful. Publication costs were paid by NASA grant 80NSSC19K1114.

Appendix A
Inertial GOL Corrections

Starting from conservation of mass in a spherically symmetric steady wind (assuming $-8 < d\ln n/d\ln r < -2$), the acceleration power law is given by

$$\begin{aligned}\frac{d\ln(nUr^2)}{d\ln r} &= 0\\ \frac{d\ln U}{d\ln r}(r) &= -\frac{d\ln n}{d\ln r}(r) - 2\\ &\simeq (8\ldots.2) - 2^{+}\\ &= +(6\ldots.0^{+}),\end{aligned} \tag{13}$$

where the range spans from near the transition region to 1 au.

Appendix B
Alternate UD Function Space: Maxwellian+Power Law Tails

The results in Equation (4) presume juxtaposed Maxwellians for the eVDF function space as shown in Figure 2. Given the large volume of 1 au electron data analyzed with the core-halo parameterization (Montgomery et al. 1968), a Maxwellian–Maxwellian eVDF function space was chosen for the experimental support by the demonstrations of the main text. The UD Maxwellian with its own e-folding provides convergent expressions for the partial density and partial pressure of the UD part of the inferred distribution function for a wide range of suprathermal parameters, including *unconstrained* UD density fractions.

By contrast, choosing a power-law model for the UD part of the eVDF *can* give similar relations, but it has artificial additional restrictions so that a finite partial pressure of the UD component precludes $\varpi \leqslant 1.1419$; this in turn precludes the UD fraction from being modeled for $\delta_F > 0.106$, which is unduly restrictive for wind core-halo data sets. These effects could be corrected using relativistic power laws at the expense of further complexity, but were not considered further.

Similar comments also make the *non-relativistic* kappa function (Olbert 1968), unattractive for the UD trial function for this modeling.

Appendix C
Difficulties Assessing δ_F from Core-halo Modeling

SERM's bookkeeping of the UD density fraction, δ_F, is based on the compartmentalization of runaway physics into two

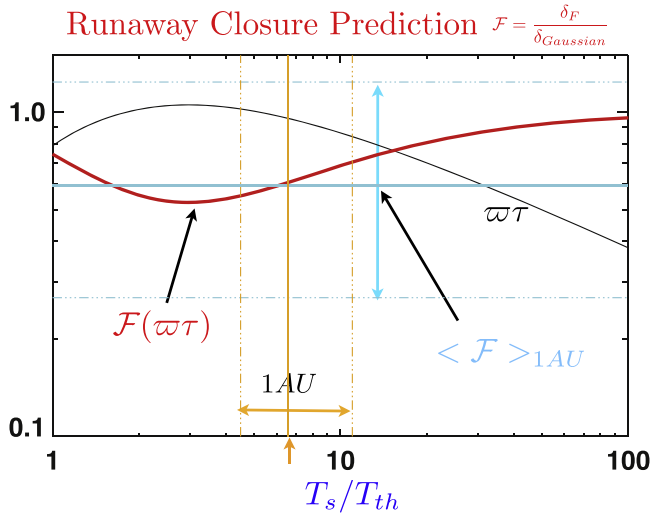

Figure 5. Ratio $\mathcal{F}$ of SERM's runaway density fraction δ_F as a fraction of the Maxwellian-fitted halo density from a fit to the same data, contrasted with this same ratio determined from 1 au data and errors (cyan) Table 1 (Feldman et al. 1979). Empirical data from Maxwellian subcomponent fits reported at 1 au (made between vertical orange dotted lines of $T_s/T_{\rm th}$). The orange arrow points at the most probable value of temperature ratio in the cited data, which, via the red $\mathcal{F}$ curve, almost exactly predicts the reported average (cyan) 1 au value of $\langle\mathcal{F}\rangle$. This ratio has been used to prepare the data theory comparison shown in Figure 1.

disjoint energy regimes. The core-halo characterization fits the observed eVDF to the *superposition* of two drifting bi-Maxwellians. This implies that *some* of the density attributed to the fitted *halo* population actually derives from phase-space density *under* that of the *core* probability distribution. Because the core occupies a sphere of radius approximately 1 halo thermal speed, this overlap is significant and must be accounted for when quantitatively making the SERM to core-halo modeling correspondence.

Theoretically the runaway fraction above ϖ is less than the "halo" Maxwellian fit density (often reported in the literature (Feldman et al. 1975) by the multiplicative factor

$$\mathcal{F}(\varpi\tau) \equiv \frac{\delta_F}{\delta_{\text{"halo"Fit}}} = \frac{2\varpi\tau e^{-\varpi^2\tau^2}}{\sqrt{\pi}} + \text{Erfc}(\varpi\tau), \tag{14}$$

illustrated in red (Figure 5) across the range of $T_s/T_{\rm th}$ that occur at 1 au. The variation of the argument $\varpi(\mathbb{E}_\parallel)\tau(\mathbb{E}_\parallel)$ in the wind data is implied by the variation of $\mathbb{E}_\parallel$ illustrated in Figure 3, which in turn implies the variation of $\tau(\mathbb{E}_\parallel)^{-2} = T_s/T_{\rm th}$ indicated in orange on the figure's lower axis. The observed mean $\langle\mathcal{F}\rangle$ and its variability (Table 1 Feldman et al. 1979) are indicated in cyan in Figure 5. This 1 au mean value $\langle\mathcal{F}\rangle \simeq 0.59$ is fully compatible with the theoretical estimate made from averaging SERM's variability of the red curve $\mathcal{F}$ over the 1 au data's horizontal variability (orange).

ORCID iDs

J. D. Scudder https://orcid.org/0000-0001-7975-5630

References

Braginskii, S. I. 1965, RvPP, 1, 205ff
Chapman, S. 1916, RSPTA, 216, 279
Chapman, S., & Cowling, T. G. 1939, Mathematical Theory of Non-uniform Gases (Cambridge: Cambridge Univ. Press)

Dreicer, H. 1959, PhRv, 115, 238
Dreicer, H. 1960, PhRv, 117, 329
Dudík, J., Dzifčáková, E., Meyer-Vernet, N., et al. 2017, SoPh, 292, 100D
Dzifčáková, E., Zemanová, A., & Dudík, J. 2018, ApJ, 853, 158D
Enskog, D. 1917, Inaugural Dissertation, Uppsala Univ.
Feldman, W. C., Asbridge, J. R., Bame, S. J., Gosling, J. T., & Lemons, D. S. 1979, JGR, 84, 7371
Feldman, W. C., Asbridge, J. R., Bame, S. J., Montgomery, M. D., & Gary, S. P. 1975, JGR, 80, 4181
Feldman, W. C., Asbridge, J. R., Bame, S. J., Montgomery, M. D., & Gary, S. P. 1978, JGR, 83, 5285
Fitzpatrick, R. 2004, Plasma Physics, An Introduction (Boca Raton, FL: CRC Press)
Fuchs, V., Cairns, R. A., Lashmore-Davies, C. N., & Shoucri, M. M. 1986, PhFl, 29, 2931
Hazeltine, R. D., & Walbroeck, F. 2004, The Framework of Plasma Physics (Boulder, CO: Westview Press)
Issautier, K., Meyer-Vernet, N., Moncuquet, M., & Hoang, S. 1998, JGR, 103, 1969
Landi, S., & Pantelinni, F. 2003, A&A, 400, 769
Marsch, E., Pilipp, W. G., Thieme, K. M., & Rosenbauer, H. 1989, JGR, 94, 6893
Meyer-Vernet, N. 2007, Basics of the Solar Wind (Cambridge: Cambridge Univ. Press), 252
Meyer-Vernet, N., Moncuquet, M., & Hoang, S. 1995, Icar, 116, 202
Montgomery, M. D., Bame, S. J., & Hundhausen, A. J. 1968, JGR, 116, 4999
Olbert, S. 1968, in Physics of the Magnetosphere, Astrophysics and Space Library, ed. R. D. L. Carovillano & J. F. McClay (Dordrecht: Reidel), 641
Olbert, S. 1983, JPL Solar Wind Five (SEE N84-13067 03-92), 149
Pannekeok, A. 1922, BAN, 1, 107
Pulupa, M., Bale, S. D., Salem, C., & Horaties, K. 2014, JGR, 119, 647
Rosenbauer, H., Schwenn, R., Marsch, E., et al. 1977, ZAGeo, 42, 561
Rosseland, S. 1924, MNRAS, 84, 720
Rossi, B., & Olbert, S. 1970, Introduction to the Physics of Space (New York: McGraw-Hill)
Scudder, J. D. 1992, ApJ, 398, 319
Scudder, J. D. 1996a, JGR, 101, 13461
Scudder, J. D. 1996b, JGR, 101, 11039
Scudder, J. D. 2019a, ApJ, in press
Scudder, J. D. 2019b, ApJ, 882, 146
Scudder, J. D. 2019c, JGR, submitted
Scudder, J. D., & Karimabadi, H. 2013, ApJ, 770, 26
Scudder, J. D., & Olbert, S. 1979, JGR, 84, 2755
Spitzer, L. J., & Harm, R. 1953, PhRv, 89, 977
Spitzer, L. J. 1962, 1967, Physics of Fully Ionized Gases (2nd ed.; New York: Wiley Interscience), 144ff
Zank, G. P. 2014, Transport Processes in Space Physics and Astrophysics (New York: Springer)